• Original Paper •

Relationships between the Extratropical ENSO Precursor and Leading Modes of Atmospheric Variability in the Southern Hemisphere

Jianhuang QIN[1], Ruiqiang DING[2,3], Zhiwei WU[*4], Jianping LI[5], and Sen ZHAO[2]

[1]*Key Laboratory of Meteorological Disaster of Ministry of Education and Earth System Modeling Center,*
Nanjing University of Information Science and Technology, Nanjing, Jiangsu 210044, China

[2]*State Key Laboratory of Numerical Modeling for Atmospheric Sciences and Geophysical Fluid Dynamics,*
Institute of Atmospheric Physics, Chinese Academy of Sciences, Beijing 100029, China

[3]*Plateau Atmosphere and Environment Key Laboratory of Sichuan Province,*
Chengdu University of Information Technology, Chengdu 610225, China

[4]*Institute of Atmospheric Sciences, Fudan University, Shanghai 200433*

[5]*College of Global Change and Earth System Sciences, Beijing Normal University, Beijing 100875, China*

ABSTRACT

Previous studies suggest that the atmospheric precursor of El Niño–Southern Oscillation (ENSO) in the extratropical Southern Hemisphere (SH) might trigger a quadrupole sea surface temperature anomaly (SSTA) in the South Pacific and subsequently influence the following ENSO. Such a quadrupole SSTA is referred to as the South Pacific quadrupole (SPQ). The present study investigated the relationships between the atmospheric precursor signal of ENSO and leading modes of atmospheric variability in the extratropical SH [including the SH annular mode (SAM), the first Pacific–South America (PSA1) mode, and the second Pacific–South America (PSA2) mode]. The results showed that the atmospheric precursor signal in the extratropical SH basically exhibits a barotropic wavenumber-3 structure over the South Pacific and is significantly correlated with the SAM and the PSA2 mode during austral summer. Nevertheless, only the PSA2 mode was found to be a precursor for the following ENSO. It leads the SPQ-like SSTA by around one month, while the SAM and the PSA1 mode do not show any obvious linkage with either ENSO or the SPQ. This suggests that the PSA2 mode may provide a bridge between the preceding circulation anomalies over the extratropical SH and the following ENSO through the SPQ-like SSTA.

Key words: Pacific–South America, atmospheric variability, ENSO, South Pacific quadrupole

1. Introduction

The El Niño–Southern Oscillation (ENSO) is the obvious climate mode of interannual Pacific sea surface temperature (SST) variability in the tropics (e.g., McPhaden et al., 2006; Deser et al., 2010). ENSO events that develop in a particular year generally reach a maximum during the following wintertime, leading to negative (La Ninã) or positive (El Niño) SST anomalies (SSTAs) in the eastern and central tropical Pacific. Despite displaying the strongest anomalies in the eastern and central tropical Pacific, ENSO can also induce divergence anomalies at the top of the troposphere over the western Pacific and the eastern Indian Ocean, which may act as potential Rossby wave sources (e.g., DeWeaver and Nigam, 2004).

The Pacific–North American (PNA) teleconnection pattern not only has an impact on the climate conditions and weather over the North Pacific and North America, but it also influences the Asian jet, Aleutian low, and the storm track over the Pacific in the Northern Hemisphere (NH) (e.g., Straus and Shukla, 2002; Compo and Sardeshmukh, 2004). The other typical wave train response to ENSO is in the Southern Hemisphere (SH), identified as the Pacific–South American (PSA) teleconnection pattern (Mo and Ghil, 1987; Karoly, 1989). The PSA pattern extends from the tropical Pacific into South America, and has an influence on the weather and climate in the SH, such as precipitation over New Zealand, the frequency of blocking in the high latitudes of the SH (Kwok and Comiso, 2002; Yuan, 2004), and the Southern Annular Mode (SAM) (e.g., L'Heureux and Thompson, 2006; Ding et al., 2012, 2015c). Thus, the energy of ENSO is transmitted from

---

* Corresponding author: Zhiwei WU
  Email: zhiweiwu@fudan.edu.cn

the low latitudes to the mid and high latitudes of the NH and the SH by PNA and PSA wave trains, allowing the influence of ENSO to extend from the tropics to the extratropics.

In addition to the influences of ENSO in extratropical regions, several previous studies have found a teleconnection between the onset of ENSO and mid-to-high latitude atmospheric variability (Vimont et al., 2003a, 2003b; Alexander et al., 2010; Ding et al., 2015a, 2015b). The dominant modes of extratropical atmospheric variability in the Pacific region are the North Pacific Oscillation mode in the NH (Walker and Bliss, 1932; Rogers, 1981) and the PSA mode in the SH (Mo and Ghil, 1987), and are characterized by large-scale sea level pressure (SLP) oscillations. Vimont et al. (2003a) identified a mechanism to explain this connection between boreal wintertime intrinsic atmospheric variability in the NH and ENSO, which they termed the seasonal footprint mechanism (SFM). The SFM suggests that NH wintertime extratropical SLP variability can impart a footprint onto the SST by changing surface heat flux, and this SST footprint persists until the following summer and can force the atmosphere in the tropics, subsequently leading to zonal wind stress anomalies along the equator. The westerly wind anomalies are conducive to generating and maintaining the intraseasonal oceanic Kelvin wave structure necessary for an ENSO event during the following boreal winter.

For the SH, Jin and Kirtman (2009) found that a wavenumber-3 structure in the extratropical South Pacific leads the maximum peak of ENSO by around three months. Ding et al. (2015a, 2015b) further analyzed the process that finally leads to an ENSO event driven by extratropical atmospheric variability during austral summer over the South Pacific. They reported that SLP variability over the South Pacific with wavenumber-3 structure may precede the maximum peak of ENSO by around one year. They suggested that this wavenumber-3 structural pattern in the South Pacific plays a significant role in the onset of ENSO events by forcing quadrapole SST variability, resembling the SFM. The discharge–recharge oscillator theory proposed by Jin (1997a, 1997b) emphasizes the role of warm water volume anomalies, which results in a self-sustained ocean–atmosphere coupled oscillation. Ding (2015a, 2015b) further indicated that the evolution of the tropical subsurface ocean temperature anomaly also has an impact on developing ENSO, resembling the trade wind feedback mechanism (Anderson et al., 2013). During austral summer the atmospheric variability over the extratropical South Pacific imparts onto the ocean a quadrapole SST anomaly (SSTA) pattern, referred to as the South Pacific quadrapole (SPQ). This SPQ-like SSTA footprint persists until austral winter and extends into the deep tropical regions, and later forces a zonal wind anomaly along the equator. Meanwhile, trade wind variability over the South Pacific induced by the wavenumber-3 structure may result in concurrent subsurface temperature and heat content anomalies in the central and eastern tropical Pacific. These two processes involving surface atmosphere–ocean coupling favor the triggering of ENSO events during the following austral summer. Ding et al. (2015b) demonstrated that South Pa-

cific extratropical forcing is relatively independent of North Pacific extratropical forcing, and they may influence the onset of ENSO events either separately or together.

A number of studies have investigated the atmospheric variability pattern in the mid–high latitudes in the South Pacific. Kidson and Renwick (2002) found two wavenumber-3 modes over the South Pacific using ECMWF reanalysis data. Mo (2000) applied empirical orthogonal function (EOF) analysis to monthly mean 500 hPa height anomalies. Results show that the first EOF mode of the austral winter (June–August) 500 hPa geopotential height is the SAM (Gong and Wang, 1999; Thompson and Wallace, 2000), and it resembles the second rotated EOF (REOF2) mode obtained by Karoly (1989) using station data. Furthermore, both the second and third EOF modes (Mo, 2000) show a wavenumber-3 pattern in quadrature with each other and a wave train with large amplitude in the PSA sector from the tropical Pacific to Argentina. In addition, Mo (2000) found that both PSA1 and PSA2 are associated with ENSO variability: the PSA1 mode is associated with a period of 40–48 months, and the PSA2 mode is associated with a period of 26 months. A recent study examined the austral winter atmospheric variability using observations and an ensemble of atmospheric model experiments (Ding et al., 2016). This study obtained three major modes by using REOF analysis. Results showed that REOF1 is linked to the SAM. In contrast, REOF2 shows a wave train associated with the concurrent western North Pacific monsoon; REOF3 is similar to the PSA pattern. Ding et al. (2015a, 2015b) showed the spatial pattern of the averaged SLP anomalies in the South and North Pacific during austral summer (November–April) regressed against the austral summertime cold tongue index. They found that an obvious wavenumber-3 structure pattern precedes ENSO by one year over the South Pacific.

These previous studies motivated us to further investigate the structure of the ENSO atmospheric precursor signal over the South Pacific and its relationships with leading modes of atmospheric variability in the extratropical SH. Specifically, we set out to discover whether the atmospheric precursor signal has analogous spatial and temporal patterns at different atmospheric levels, which leading modes have relationships with the ENSO atmospheric precursor signal, and whether the canonical SAM or PSA pattern may be an atmospheric precursor signal of ENSO. Following this introduction, section 2 describes the data; in section 3 we investigate the ENSO atmospheric precursor signal in the SH; section 4 shows the difference between the ENSO atmospheric precursor signal and the three leading modes of atmospheric variability; and section 5 summarizes and discusses the major results of the study.

2. Datasets

The SST data used in this study are from the Hadley Centre Sea Ice and SST (HadISST) dataset for the period 1950–2010, which has a horizontal resolution of $1° \times 1°$

(Rayner et al., 2006). We used the National Centers for Environmental Prediction–National Center for Atmospheric Research (NCEP–NCAR) atmospheric circulation reanalysis (Kalnay et al., 1996), including SLP, 200–850 hPa geopotential height and surface winds for the period 1950–2010 on a $2.5° \times 2.5°$ grid. We calculated the monthly anomalies by subtracting the climatological mean annual cycle. Note that we define austral summer as December–January–February (DJF), although when referring to the results of Ding et al. (2015b), austral summer covers November–April. Relative to a given year (0) we refer to preceding and following years as (−1) and (+1), respectively.

In this study, ENSO is indicated by the Niño-3, Niño3.4 and Niño4 indices, derived from SSTA estimates in the Niño3 region (5°N–5°S, 150°–90°W), Niño3.4 region (5°N–5°S, 170°–120°W) and Niño4 region (5°N–5°S, 160°–150°W), respectively. The Niño indices were extracted from the Climate Prediction Center of the National Oceanic and Atmospheric Administration (NOAA).

3. Atmospheric precursor signal preceding ENSO by one year

Ding et al. (2015b) showed the regressed spatial structure of the November–April austral summer (+1)-averaged cold tongue index on the austral summer SLP anomalies (0) during the preceding year in the Pacific. They found a wave train from the midlatitude southwestern Pacific to the southwest coast of Argentina with three centers of SLP anomalies. Further studies by the same authors confirmed that this wave train over the South Pacific may be an atmospheric precursor signal preceding ENSO by around one year in the SH. They then defined the ENSO atmospheric precursor signal index as the averaged normalized SLP anomaly difference between the positive center (72°–52°S, 177°–130°W) and the sum of the two negative centers [(48°–25°S, 155°E–145°W) and (57°–33°S, 110°–75°W)].

To investigate the spatial and temporal patterns of the ENSO atmospheric precursor signal at different levels, we followed Vimont et al. (2003a, 2003b) by performing a singular value decomposition [SVD; also known as maximum covariance analysis (Bretherton et al., 1992)] on austral summer (0) South Pacific extratropical geopotential heights (850 hPa, 700 hPa, 500 hPa, and 200 hPa) for the period 1950–2010, and SLP (south of 20°S) against austral summer (+1) tropical Pacific SST (DJF) (i.e., one year later than the extratropical geopotential heights and SLP), respectively. Similar results were obtained when we considered different pressure levels (see Table 1). The time series of heterogeneous geopotential height and SLP fields at the five different levels are similar and the correlations between the different levels are significant at the 99% level, and the correlations vary between 0.64 and 0.98.

The spatial and temporal modes of the 500 hPa geopotential height data and SST data used to generate the SVD

Table 1. Correlation between the SVD leading normalized expansion coefficients of the austral summer 200 hPa, 500 hPa, 700 hPa, 850 hPa geopotential height field and SLP (not shown). All these correlations are significant at or above the 99% level.

	200 hPa	500 hPa	700 hPa	850 hPa	SLP
200 hPa	–	0.78	0.78	0.74	0.69
500 hPa	–	–	0.85	0.76	0.64
700 hPa	–	–	–	0.98	0.91
850 hPa	–	–	–	–	0.98
SLP	–	–	–	–	–

are shown in Fig. 1. The leading SVD mode [between austral summer (0) extratropical 500 hPa geopotential height in the SH and the following austral summer (+1) tropical Pacific SST] for the period 1950–2010 explains 56% of the total squared covariance. These two corresponding expansion coefficient time series are shown in Fig. 1c, and the correlation coefficient between the two time series is 0.67 for the period 1950–2010, which is significant at the 0.001 level. The leading pair of heterogeneous patterns is shown in Fig. 1a and b, obtained by calculating the correlation of the heterogeneous 500 hPa geopotential height and SST with the two SVD leading normalized time series, respectively. The austral summer (0) South Pacific 500 hPa geopotential height has a marked wave train with a wavenumber-3 pattern from the midlatitude southwestern Pacific to Argentina. A "seesaw" in the SST is shown in Fig. 1b, which is dominated by negative anomalies in the western tropical Pacific and positive anomalies in the eastern tropical Pacific during the following austral summer (+1). This means that the SST pattern for the period 1950–2010 bears a resemblance to ENSO. The SVD results show that the ENSO atmospheric precursor signal linked to ENSO during the following austral summer (+1) event represents a wavenumber-3 pattern at different levels, which means the ENSO atmospheric precursor signal has an equivalent barotropic structure over the South Pacific during austral summer.

Next, a simple index that measures the variability in the ENSO atmospheric precursor 500 hPa geopotential height anomalies pattern over the South Pacific (hereafter referred to as the South Pacific index, SPI) was constructed by taking the difference between the normalized 500 hPa heterogeneous geopotential height anomalies averaged over the positive center (175°–140°W, 70°–60°S) and the sum of the normalized 500 hPa heterogeneous geopotential height anomalies averaged over the two negative centers of (50°–37°S, 150°E–180°) and (50°–30°S, 120°–90°W), as shown in Fig. 1a. We note that the correlation coefficient of the SPI based on 500 hPa geopotential height and the index defined by Ding et al. (2015b) based on SLP is strong (0.88) for the period 1950–2010 during austral summer.

Figure 2a shows the regression of the 500 hPa geopotential height anomalies during austral summer (DJF-averaged) on the concurrent austral summer SPI for the period 1950–2010. We note that this 500 hPa geopotential height pattern resembles the PSA2 pattern shown in Fig. 1 of Mo (2000).
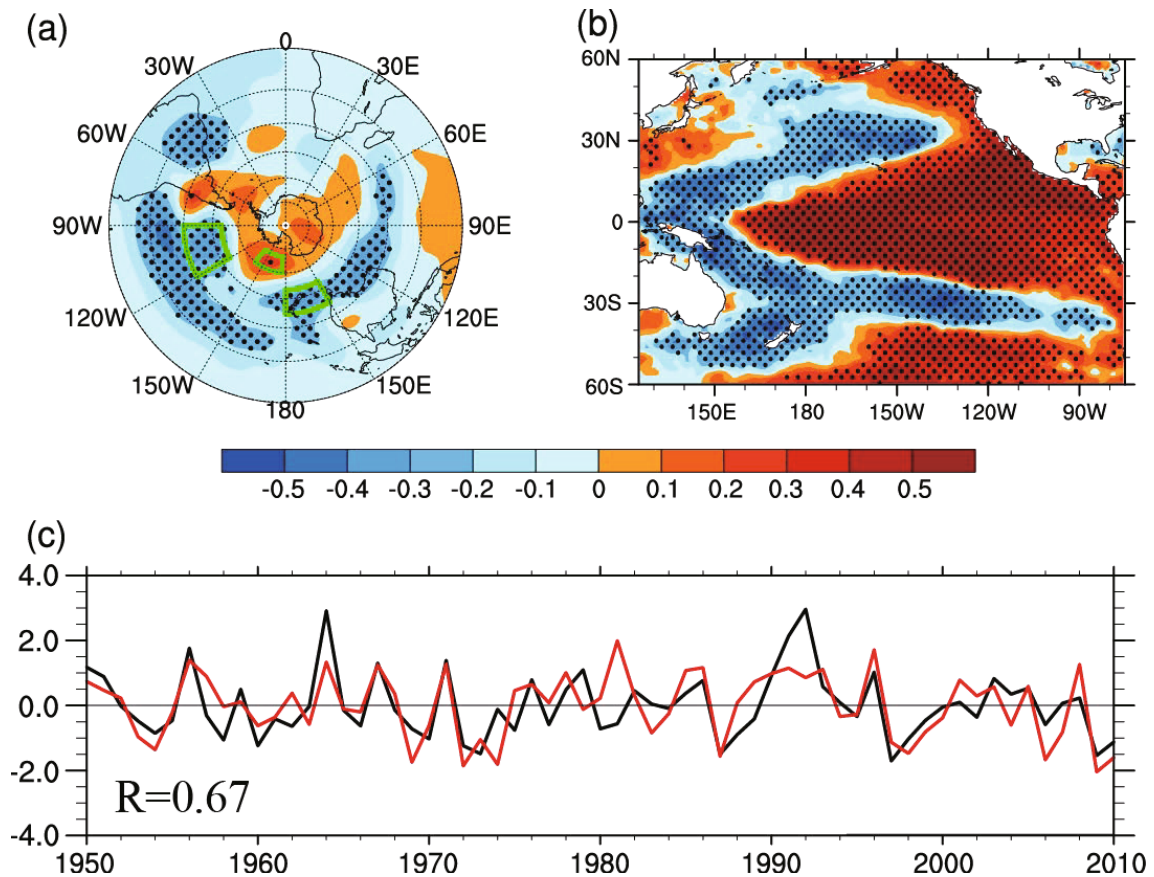
Fig. 1. Spatial properties of the leading SVD mode for (a) the previous austral summer (0) (DJF-averaged) Southern Hemisphere (90°–20°S) 500 hPa geopotential height anomalies and (b) the austral summer (+1) (DJF-averaged) tropical Pacific (20°S–20°N, 125°E–75°W) SSTAs, shown as correlation maps of the respective heterogeneous 500 hPa geopotential height anomalies and SST fields with the SVD leading expansion coefficients. (c) The SVD leading normalized expansion coefficients of the austral summer (0) 500 hPa geopotential height field (black line) and the following austral summer (+1) tropical Pacific SST field (red line). In (a) and (b), areas with correlation significant at or above the 90% level are shaded. In (a), three green boxes [positive regression box: (70°–60°S, 175°–140°W); negative regression boxes: (50°–37°S, 150°E–180°) and (50°–30°S, 120°–90°W)] indicate the locations of three action centers of the ENSO precursor.

Furthermore, Seager et al. (2003) and L'Heureux and Thompson (2006) demonstrated that the extratropical atmospheric variability response in the SH to tropical SST forcing produces a PSA-like wave train but with a strong zonal mean structure during austral summer. This 500 hPa geopotential height pattern is regarded as the PSA2 pattern. These results are also consistent with Jin and Kirtman (2009) and Ding et al. (2015a, 2005b). Both Fig. 1a and Fig. 2a show that the ENSO atmospheric precursor signal in the SH has a wavenumber-3 pattern over the South Pacific.

4. Relationships

4.1. *Relationships between the ENSO atmospheric precursor signal and leading modes of atmospheric variability*

To further explore the spatial structure and temporal variation of the ENSO atmospheric precursor signal over the South Pacific, we compare the atmospheric precursor signal with the three leading modes of atmospheric variability in the SH. The canonical SAM and PSA patterns are usually obtained from EOF analysis of the SH monthly 500 hPa geopotential height anomalies (Mo, 2000). The first three leading EOF modes of the monthly 500 hPa geopotential height anomalies in the SH poleward of 20°S (after removing the monthly mean global average geopotential height anomalies) for the period 1950–2010 are presented in Figs. 3a–c. EOF1, EOF2, and EOF3 account for 21.6%, 12.2%, and 10.5% of the extratropical SH 500 hPa geopotential height variability, respectively. The EOF1 pattern (Fig. 3a) is the SAM, which is a dominant mode of atmospheric variability in the SH. The EOF2 and EOF3 patterns are respectively referred to as PSA1 and PSA2. Moreover, their phases are almost in quadrature, and display a zonal wavenumber-3 structure from the tropical Pacific to Argentina (Figs. 3b and c).

Correlations between the austral summer SPI and the time series of the three leading modes are shown in Figs. 3d–f.
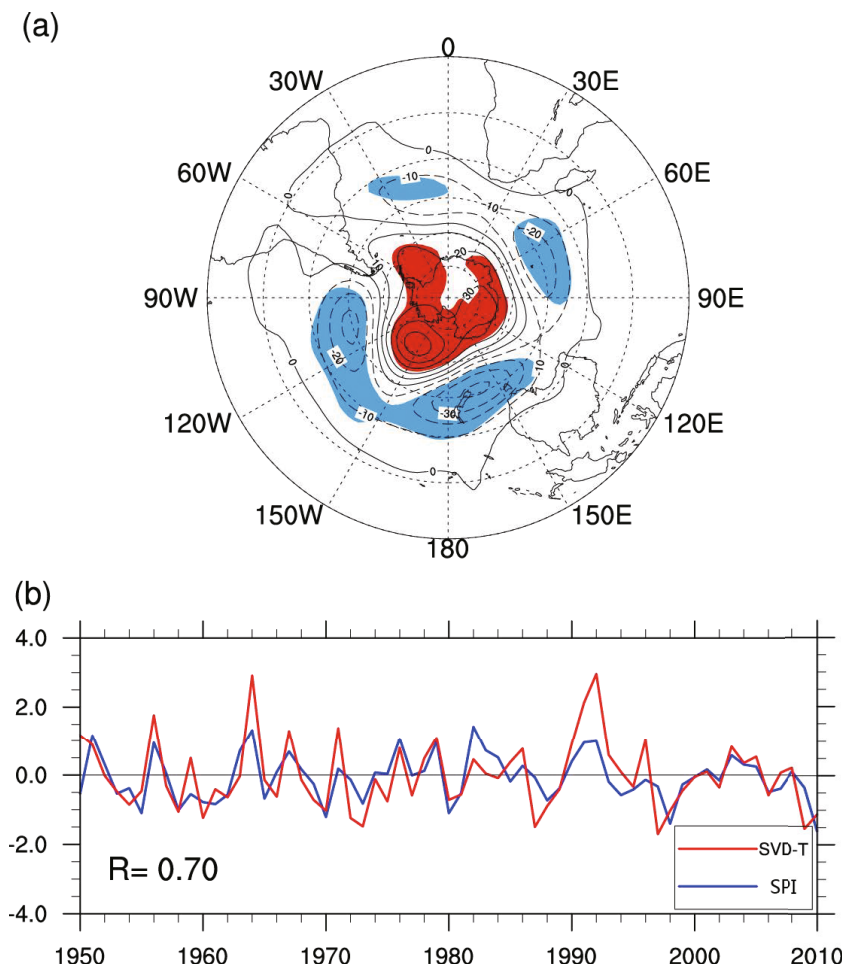
(a)

(b)

Fig. 2. (a) Regression of the austral summer (DJF-averaged) 500 hPa geopotential height anomalies on the austral summer SPI for the period 1950–2010. Positive (red) and negative (blue) 500 hPa geopotential height anomalies, significant at the 90% level, are shaded. (b) Coefficients of index obtained by SVD (red line) and SPI (blue line).

The time series of the three leading modes are known as the SAM index, the PSA1 index, and the PSA2 index, respectively. The correlation of the SPI with the PSA2 index is 0.56 (significant at the 99.9% confidence level, Fig. 3f), which is slightly greater than the correlation ($R = 0.47$; also significant at the 99.9% confidence level) of the SPI with the SAM index during austral summer (Fig. 3d). In contrast, the correlation of the SPI and the PSA1 index is only 0.13 (not significant even at the 90% confidence level) during austral summer for the period 1950–2010. This result means that the SPI has the strongest relationship with the PSA2 index, but it is also significantly correlated with the SAM index during austral summer.

To quantify the linkage between the ENSO atmospheric precursor signal and the three leading modes during austral summer, we followed the approach that can be referred to in Newman et al. (2003) and Schneider and Cornuelle (2005), and assumed that the change in the austral summer ENSO atmospheric precursor signal depends on an autoregressive model of order 1: Eq. (1) shows that the first, second and third terms on the right-hand side mean the terms associated

with the SAM, PSA1 and PSA2, and η is uncorrelated noise.

$$\text{SPI} = \alpha\text{SAM} + \beta\text{PSA1} + \gamma\text{PSA2} + \eta . \qquad (1)$$

The coefficients $\alpha = 0.36$, $\beta = 0.39$, and $\gamma = 0.75$ were obtained from observations by regressing the SPI against the values of SAM, PSA1, and PSA2 for the same months, respectively. The regression of reconstructed austral summer (DJF-averaged) SPI obtained from Eq. (1) against 500 hPa geopotential height anomalies during austral summer is shown in Fig. 4. Both the spatial mode of the reconstructed pattern and the raw ENSO atmospheric precursor signal pattern (Figs. 1a and 2a) have a wavenumber-3 structure over the South Pacific. In addition, the reconstructed SPI has a strong correlation with the SPI ($R = 0.7$).

4.2. *Lead–lag relationships with ENSO*

In section 4.1 we found that the ENSO atmospheric precursor signal mainly has obvious correlations with the SAM and PSA2 modes during austral summer. But do these two leading modes play an important role as an atmospheric precursor signal in triggering ENSO? To address this question,
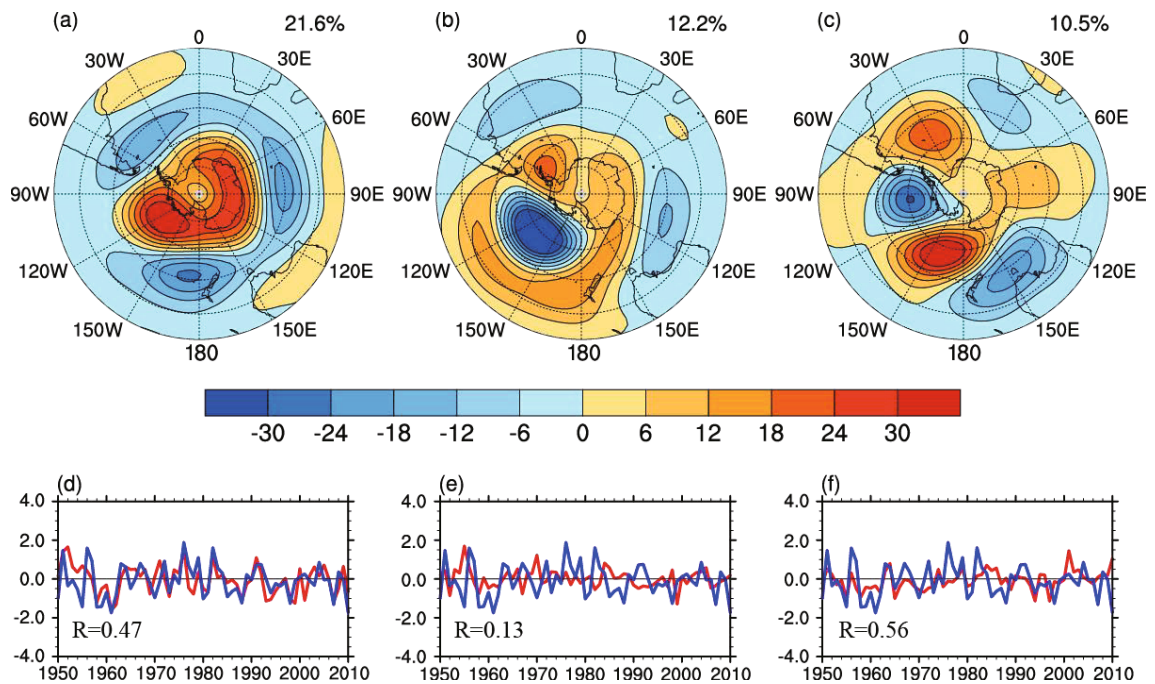
Fig. 3. Spatial patterns of (a) EOF1, (b) EOF2, and (c) EOF3 of the monthly 500 hPa geopotential height field over the SH poleward of 20°S for the period 1950–2010 (after removing the monthly mean global average geopotential height anomalies). Time series of the austral summer (DJF) SPI (blue line) overlaid with (d) the PC1 (red line), (e) the PC2 (red line), and (f) the PC3 (red line).
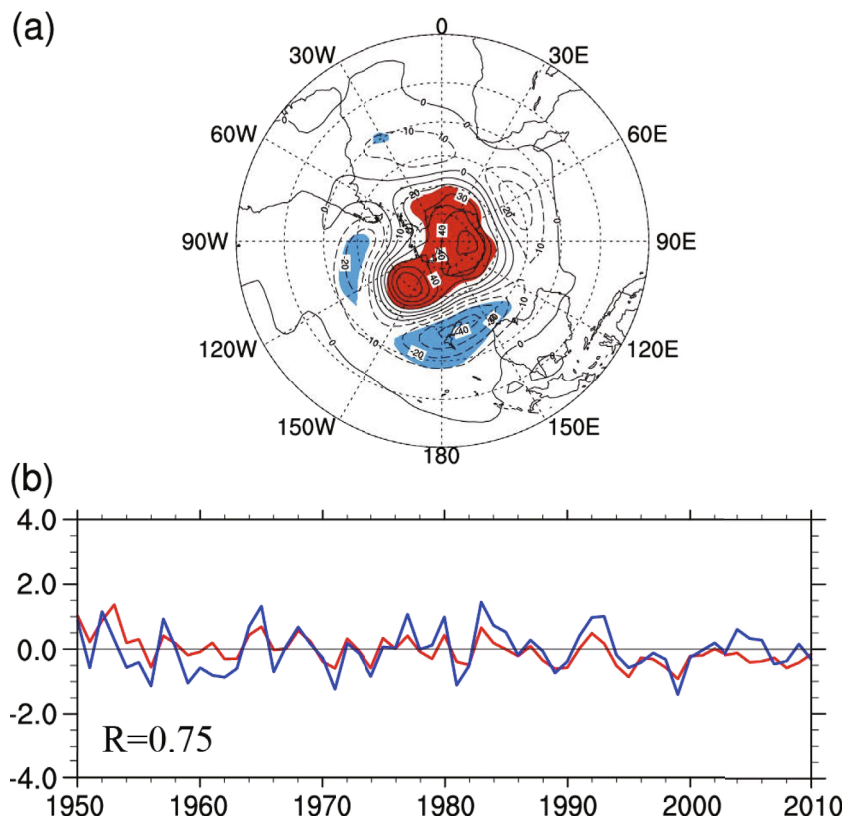

Fig. 4. The regression of reconstructed austral summer (DJF-averaged) SPI obtained from Eq. (1) against 500 hPa geopotential height anomalies. Positive (red) and negative (blue) 500 hPa geopotential height anomalies, significant at the 90% level, are shaded. (b) Observed (blue line) and reconstructed (red line) SPI using an autoregressive model consisting of the EOFs. The correlation coefficient (*R*) between the monthly values of observed and reconstructed PSA indices is given in the lower left corner.

we show in Fig. 5 the lead–lag correlations of the SPI, SAM, PSA1 and PSA2 indices with the three-month running Niño indices (including the Niño1+2, Niño3, Niño4 and Niño3.4 indices). The results show that the peak correlations ($R = 0.25$ and 0.28; both significant at the 0.1 level) of the SAM and PSA1 indices with all Niño indices occur at the 0 time lag (Figs. 5a and b). For lead times, the SAM and PSA1 indices exhibit weak correlations with the Niño indices from a few months to around one year. In contrast, the peak correlations ($R = 0.35$ and 0.29; both significant at the 0.01 level) of the SPI and PSA2 index with all Niño indices occur when the SPI and PSA2 index lead the Niño indices by 12–15 months (Figs. 5c and d). These results suggest that only the PSA2 pattern tends to have a close connection with ENSO more than one year later (similar to the SPI).

To further illustrate the relationships between the three leading modes and ENSO, we carried out regression analysis of the austral summer (0) (DJF) SSTA on the austral summer (−1) SPI, SAM, PSA1, and PSA2 indices, separately (Figs. 6a–d). It is evident that the PSA2-related SST pattern one year later is similar to the SST pattern associated with the SPI one year later. Figures 6a and d show that positive SSTAs exist in the central and eastern tropical Pacific and negative SSTAs exist in the western tropical Pacific, thereby representing a pronounced ENSO-like pattern in the tropical Pacific. However, during the following austral summer, the SSTAs (especially the positive SSTAs) linked to the previous austral summer (−1) SAM and PSA1 are weakest in the tropical Pacific, resulting in negligible SSTAs there (Figs. 6b and c).

Figure 7 shows a partial regression analysis of the austral summer SPI on the following austral summer SSTAs with the DJF-averaged SAM index, PSA1 index, and PSA2 index

removed. With the SAM and PSA1 indices removed, regressions are not substantially reduced in most areas of the tropics and an obvious El Niño pattern remains. In contrast, regressions are remarkably reduced in most areas of the tropical Pacific and the El Niño pattern becomes indistinct after the PSA2 signal is removed from the SPI. These results indicate that the PSA2 (not the SAM and PSA1) plays an important role in linking the ENSO extratropical atmospheric precursor signal to the following austral summer ENSO. Therefore, we should investigate the role of the PSA2 in the process by which the extratropical atmospheric precursor signal triggers ENSO events.

4.3. *Lead–lag relationships with the SPQ*

According to Ding et al. (2015a, 2015b), surface heat flux anomalies display a quadrapole-like pattern forced by anomalous surface winds, which is linked to the atmospheric variability in the SH, and this quadrapole-like pattern in turn motivates an quadrapole SST pattern (SPQ) onto the ocean; the SPQ, as an ocean bridge, subsequently has an influence on the onset of ENSO via atmosphere–ocean coupling in the subtropical South Pacific. Ding et al. (2015a, 2015b) further found that the ENSO atmospheric precursor signal in the SH leads the SPQ pattern by one month, and the atmospheric variability with wavenumber-3 structure forces approximately 50% of the SPQ variability.

To examine the relationship between the PSA2 mode and SPQ, we regressed the PSA2 index onto the January–March (JFM)-averaged SSTAs (Fig. 8a). The one-month lag SST pattern shows an SPQ-like SSTA pattern in the extratropical South Pacific. Furthermore, Fig. 8b shows the lead–lag correlations between the DJF-averaged PSA2 and the monthly SPQ index. The SPQ index was obtained from Ding et al.
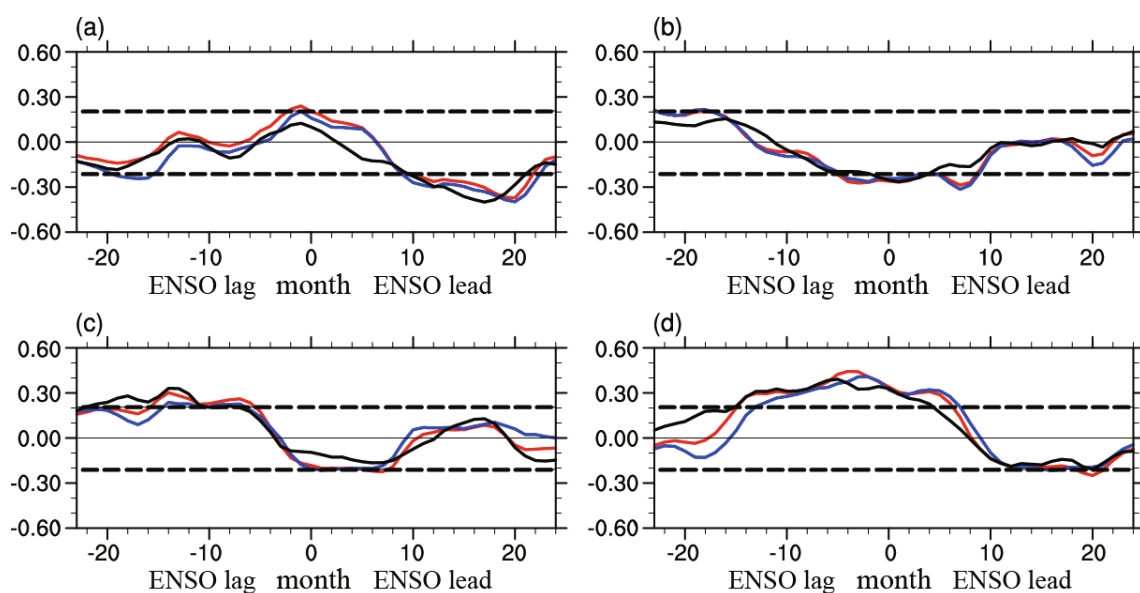

Fig. 5. Lead–lag correlation coefficients between the monthly Niño indices, including Niño3 (blue line), Niño4 (black line), and Niño3.4 (red line), and the austral summer (DJF-averaged) (a) SAM index, (b) PSA1 index, (c) PSA2 index, and (d) SPI. The horizontal dashed line shows the 0.1 significance level.
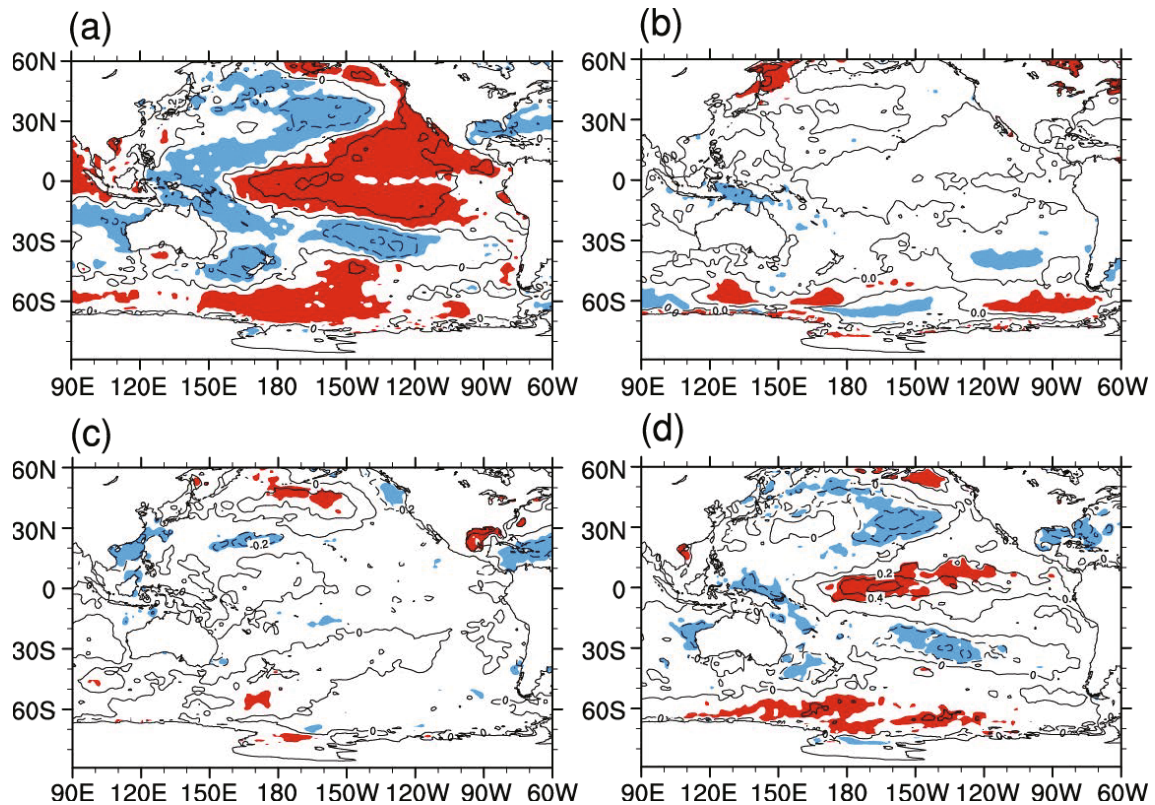
Fig. 6. Regression of the following austral summer (DJF-averaged) SST anomalies on the austral summer (a) SPI, (b) SAM index (obtained from Fig. 4d), (c) PSA1 index (obtained from Fig. 4d), and (d) PSA2 index (obtained from Fig. 4e). Positive (red) and negative (blue) SST anomalies, significant at the 90% level, are shaded.

(2015b), who defined the SPQI as the averaged normalized SST anomaly difference between the sum of the two positive centers [(58°–36°S, 173°–145°W) and (37°–17°S, 103°–76°W)] and the sum of the two negative centers [(47°–25°S, 142°E–179°W) and (59°–40°S, 113°–81°W)]. The highest correlation ($R = 0.54$, significant at the 0.001 level) occurs when the PSA2 index leads the SPQI by one month, indicating a significant influence of the atmosphere on the ocean. The above results suggest that the PSA2 may be an important part of the atmospheric signal in forcing the SPQ pattern, and the latter forces the equatorial westerly wind anomalies that finally trigger an ENSO event.

5. Summary and discussion

In this study, we examined the connection between extratropical South Pacific atmospheric variability and ENSO to discover the spatial patterns of atmospheric circulation anomaly patterns over the SH preceding ENSO by one year. We conclude that a wavenumber-3 structure of atmospheric circulation anomalies over the South Pacific may be considered as the atmospheric precursor signal of ENSO in the SH. The results are consistent with those of Ding et al. (2015b), who confirmed a lagged relationship between ENSO and atmospheric variability in the SH.

To further elucidate the relationship between the ENSO

atmospheric precursor signal and the leading modes of atmospheric variability in the SH, we obtained the canonical SAM and PSA patterns based on an EOF analysis of the SH monthly 500 hPa geopotential height anomalies (Mo, 2000). The three EOF leading modes correspond to the SAM and two PSA patterns. The results suggest that the spatial pattern of the ENSO atmospheric precursor signal during austral summer is similar to a PSA2-type wave train over the South Pacific but with a zonal mean structure. The correlations of the ENSO atmospheric precursor signal with SAM and PSA2 are important at or above the 99% confidence level, but the correlation between the ENSO atmospheric precursor signal and PSA2 is higher than that between the ENSO atmospheric precursor signal and SAM during austral summer for the period 1950–2010.

To further investigate the role of atmospheric variability in triggering the onset of ENSO, we calculated lead–lag correlations between all austral summer Niño indices and the SAM, PSA1, and PSA2 indices. The results indicated that PSA2 displays stronger correlations with the Niño indices than do the SAM and PSA1 for lead times of 12–15 months. Regression analysis of the following austral summer SST variability on the SAM, PSA1, and PSA2 indices showed that only PSA2 may be associated with the ENSO-like SST pattern during the following austral summer. Partial regression analysis showed similar conclusions; that is, the PSA2 is associated with ENSO, while the SAM and PSA1 do not have
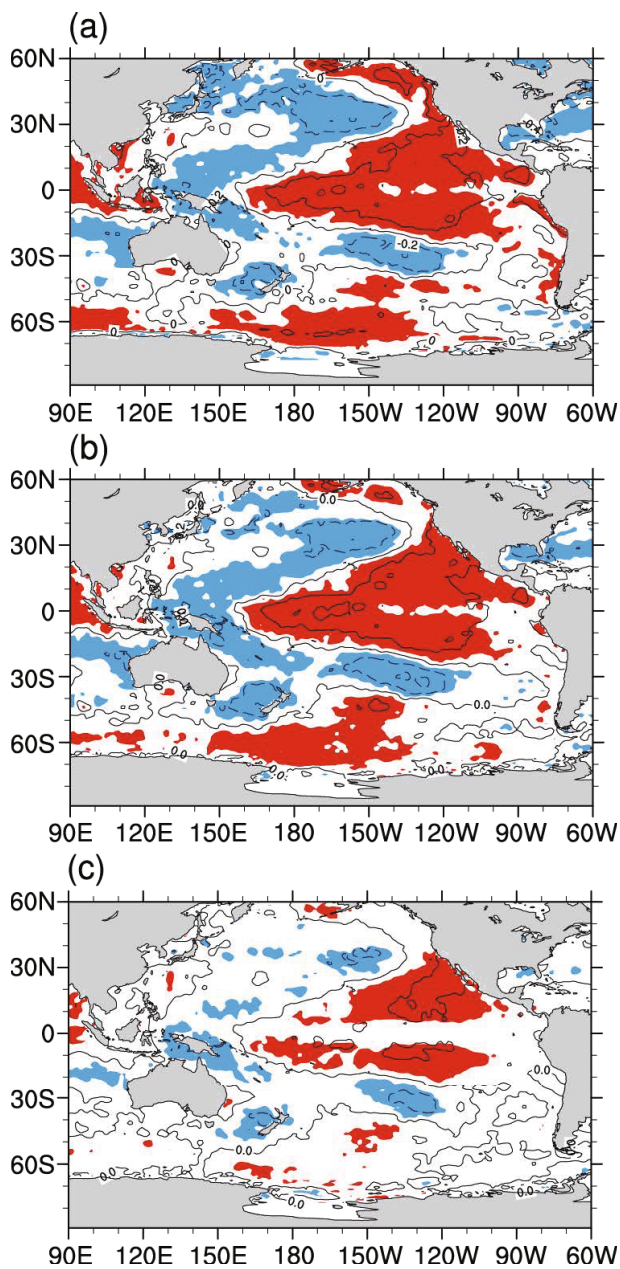
Fig. 7. Regression of austral summer (DJF-averaged) SST anomalies on the austral summer SPI, (a) with SAM index removed, (b) with PSA1 index removed, and (c) with PSA2 index removed.

Fig. 8. (a) Regression of the JFM-averaged SST anomalies on the austral summer PSA2 index (obtained from Fig. 4e). Positive (red) and negative (blue) SST anomalies, significant at the 90% level, are shaded. (b) Lead–lag correlation coefficients of the austral summer (DJF-averaged) PSA2 index and 3-month running SPQI. In (a), the four green boxes [positive regression boxes: (58°–36°S, 173°–145°W) and (37°–17°S, 103°–76°W); negative regression boxes: (47°–25°S, 142°E–179°W) and (59°–40°S, 113°–81°W)] defined the SPQI. In (b), the horizontal dashed lines show the 0.1, 0.05 and 0.01 significance levels.

a significant leading correlation with ENSO.

Previous studies suggest that anomalous surface winds linked to the atmospheric variability in the SH can force a quadrapole SST pattern by forcing a quadrapole-like pattern on the surface heat flux anomalies in the South Pacific (Ding et al., 2016); the SPQ, as an ocean bridge, subsequently has an influence on the onset of ENSO via atmosphere–ocean coupling in the subtropical South Pacific. To confirm that PSA2 plays a role in the onset of ENSO, we examined the relationship between PSA2 and SPQ. The analysis indicated that the austral summer PSA2 leads SPQ by one month, and
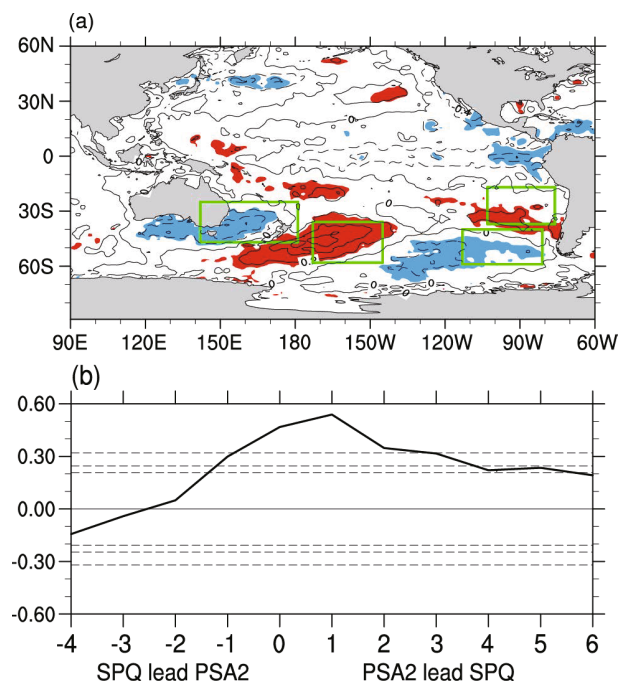
PSA2 is associated with a quadrapole-like SST pattern during JFM.

The findings of this study emphasize the role played by South Pacific extratropical forcing in ENSO variability. However, a few studies have indicated that tropical variability has an influence on extratropical atmospheric variability in the SH. Mo and Paegle (2001) found that both PSA modes (including the PSA1 and the PSA2 modes) are influenced by the Madden–Julian Oscillation. Ding et al. (2012) found that, although the SAM is an intrinsic pattern of atmospheric variability in the SH, the SAM index represents the combination of both tropically forced variability and high-latitude atmospheric variability. It remains to be explained whether the atmospheric precursor signal is an intrinsic mode of atmospheric variability in the SH or tropically forced variability. Further study is required in this regard. In addition, the present study did not consider the reasons why the ENSO atmospheric precursor signal has a high correlation with the SAM during austral summer. Pursuit of this question will require further analysis of the influence of the SAM on the linkage between the atmospheric precursor signal and ENSO. The present research is an empirical study based on observational data; modeling studies are essential to reach

more definite conclusions on the process that triggers ENSO events. Additional analysis founded on simulations in coupled atmosphere–ocean models is necessary to elucidate the process by which the extratropical forcings over the South Pacific influence ENSO.

Boschat et al. (2013) demonstrated that extratropical SST (including the North Pacific, South Atlantic, and South Indian oceans) may offer some significant information on the prediction of ENSO during late boreal winter. This new precursor signal (named "combined" SST) is most significantly consistent with the Niño3.4 SST time series and provides some potential value in the forecast of ENSO events. In addition, Ding et al. (2015b) proposed an empirical forecast model of the Niño3.4 index during boreal winter (+1) by using a linear regression method based on both SPQ and VM indices during the boreal winter (0) [Victoria mode, the ENSO precursor signal in North Pacific SST (Vimont et al., 2003a, 2003b; Alexander et al., 2010; Yu and Kim, 2011)]. The results showed that the correlation skill can reach 0.65 when using both the SPQ and VM indices to forecast the following boreal winter Niño3.4 index, and this correlation is higher than the correlation achieved by using only the SPQ or VM to hindcast the following Niño3.4 index. These studies suggest that these South or North Pacific extratropical SST precursor signals do indeed provide useful information for the prediction of subsequent ENSO events. Further analysis of the skill of ENSO prediction with the influence of the South Pacific is needed in future research.

REFERENCES

Alexander, M. A., D. J. Vimont, P. Chang, and J. D. Scott, 2010: The impact of extratropical atmospheric variability on ENSO: Testing the seasonal footprinting mechanism using coupled model experiments. *J. Climate*, **23**, 2885–2901.

Anderson, B. T., R. C. Perez, and A. Karspeck, 2013: Triggering of El Niño onset through trade wind-induced charging of the equatorial Pacific. *Geophys. Res. Lett.*, **40**, 1212–1216, doi: 10.1002/grl.50200.

Boschat, G., P. Terray, and S. Masson, 2013: Extratropical forcing of ENSO. *Geophys. Res. Lett.*, **40**(8), 1605–1611.

Bretherton, C. S., C. Smith, and J. M. Wallace, 1992: An intercomparison of methods for finding coupled patterns in climate data. *J. Climate*, **5**, 541–560.

Compo, G. P., and P. D. Sardeshmukh, 2004: Storm track predictability on seasonal and decadal scales. *J. Climate*, **17**, 3701–3720.

Deser, C., M. A. Alexander, S. P. Xie, and A. S. Phillips, 2010: Sea surface temperature variability: Patterns and mechanisms. *Annual Review of Marine Science*, **2**, 115–143.

DeWeaver, E., and S. Nigam, 2004: On the forcing of ENSO teleconnections by anomalous heating and cooling. *J. Climate*, **17**, 3225–3235.

Ding, H., R. J. Greatbatch, and G. Gollan, 2015c: Tropical impact on the interannual variability and long-term trend of the Southern Annular Mode during austral summer from 1960/1961 to 2001/2002. *Climate Dyn.*, **44**, 2215–2258.

Ding, H., R. J. Greatbatch, H. Lin, F. Hansen, G. Gollan, and T. Jung, 2016: Austral winter external and internal atmospheric variability between 1980 and 2014. *Geophys. Res. Lett.*, **43**, 2234–2239, doi: 10.1002/2016GL067862.

Ding, Q. H., E. J. Steig, D. S. Battisti, and J. M. Wallace, 2012: Influence of the tropics on the Southern Annular Mode. *J. Climate*, **25**(18), 6330–6348.

Ding, R. Q., J. P. Li, Y. H. Tseng, C. Sun, and Y. P. Guo, 2015a: The Victoria mode in the North Pacific linking extratropical sea level pressure variations to ENSO. *J. Geophys. Res.*, **120**, 27–45, doi: 10.1002/2014JD022221.

Ding, R. Q., J. P. Li, and Y. H. Tseng, 2015b: The impact of South Pacific extratropical forcing on ENSO and comparisons with the North Pacific. *Climate Dyn.*, **44**, 2017–2034.

Gong, D. Y., and S. W. Wang, 1999: Definition of Antarctic oscillation index. *Geophys. Res. Lett.*, **26**, 459–462, doi: 10.1029/1999GL900003.

Jin, D., and B. P. Kirtman, 2009: Why the Southern Hemisphere ENSO responses lead ENSO. *J. Geophys. Res.*, **114**, D23101.

Jin, F. F., 1997a: An equatorial ocean recharge paradigm for ENSO. Part I: Conceptual model. *J. Atmos. Sci.*, **54**, 811–829.

Jin, F. F., 1997b: An equatorial ocean recharge paradigm for ENSO. Part II: A stripped-down coupled model. *J. Atmos. Sci.*, **54**, 830–847.

Kalnay, E., and Coauthors, 1996: The NCEP/NCAR 40-year reanalysis project. *Bull. Amer. Meteor. Soc.*, **77**, 437–471.

Karoly, D. J., 1989: Southern Hemisphere circulation features associated with El Niño-Southern Oscillation events. *J. Climate*, **2**, 1239–1252.

Kidson, J. W., and J. A. Renwick, 2002: The southern hemisphere evolution of ENSO during 1981–99. *J. Climate*, **15**, 847–863.

Kwok, R., and J. C. Comiso, 2002: Southern Ocean climate and sea ice anomalies associated with the Southern Oscillation. *J. Climate*, **15**, 487–501.

L'Heureux, M. L., and D. W. J. Thompson, 2006: Observed relationships between the El Niño-Southern Oscillation and the extratropical zonal-mean circulation. *J. Climate*, **19**, 276–287.

McPhaden, M. J., S. E. Zebiak, and M. H. Glantz, 2006: ENSO as an integrating concept in earth science. *Science*, **314**, 1740–1745.

Mo, K. C., 2000: Relationships between low-frequency variability in the Southern Hemisphere and sea surface temperature anomalies. *J. Climate*, **13**, 3599–3610.

Mo, K. C., and M. Ghil, 1987: Statistics and dynamics of persistent anomalies. *J. Atmos. Sci.*, **44**, 877–901.

Mo, K. C., and J. N. Paegle, 2001: The Pacific-South American modes and their downstream effects. *International Journal of Climatology*, **21**(10), 1211–1229.

Newman, M., G. P. Compo, and M. A. Alexander, 2003: ENSO-forced variability of the Pacific decadal oscillation. *J. Climate*, **16**, 3853–3857.

Rayner, N. A., P. Brohan, D. E. Parker, C. K. Folland, J. J.

Kennedy, M. Vanicek, T. J. Ansell, and S. F. B. Tett, 2006: Improved analyses of changes and uncertainties in sea surface temperature measured in situ since the mid-nineteenth century: The HadSST2 dataset. *J. Climate*, **19**, 446–469.

Rogers, J. C., 1981: The North Pacific oscillation. *J. Climatol.*, **1**, 39–57.

Schneider, N., and B. Cornuelle, 2005: The forcing of the Pacific decadal oscillation. *J. Climate*, **18**, 4355–4373.

Seager, R., N. Harnik, Y. Kushnir, W. Robinson, and J. Miller, 2003: Mechanisms of hemispherically symmetric climate variability. *J. Climate*, **16**, 2960–2978.

Straus, D. M., and J. Shukla, 2002: Does ENSO force the PNA. *J. Climate*, **15**, 2340–2358.

Thompson, D. W. J., and J. M. Wallace, 2000: Annular modes in the extratropical circulation. Part I: Month-to-month variabil-

ity. *J. Climate*, **13**, 1000–1016.

Vimont, D. J., D. S. Battisti, and A. C. Hirst, 2003b: The seasonal footprinting mechanism in the CSIRO general circulation models. *J. Climate*, **16**, 2653–2667.

Vimont, D. J., J. M. Wallace, and D. S. Battisti, 2003a: The seasonal footprinting mechanism in the Pacific: Implications for ENSO. *J. Climate*, **16**, 2668–2675.

Walker, G. T., and E. W. Bliss, 1932: World weather V. *Memoirs of the Royal Meteorological Society*, **4**, 53–84.

Yu, J. Y., and S. T. Kim, 2011: Relationships between extratropical sea level pressure variations and the central Pacific and eastern Pacific types of ENSO. *J. Climate*, **24**, 708–720.

Yuan, X. J., 2004: ENSO-related impacts on Antarctic sea ice: A synthesis of phenomenon and mechanisms. *Antarctic Science*, **16**, 415–425.